Supporting Information

Atomistic Structures of Zeolite-Templated Carbon

Erin E. Taylor, Kaitlin Garman, and Nicholas P. Stadie*

Department of Chemistry & Biochemistry, Montana State University, Bozeman, Montana, 59717, United States

*Corresponding author: nstadie@montana.edu

Contents:

1. Experimental Methods

1.1. ZTC Synthesis: The zeolite NaY template (2 g, HSZ 320NAA, Tosoh Corp.) was degassed in a 2-neck round-bottom flask at 300 °C for 24 h under oil-free vacuum ($<2 \times 10^{-3}$ mbar). The dried zeolite was then combined with 20 mL of furfuryl alcohol (FA, 99%, Aldrich) via syringe and the mixture was stirred at room temperature for 24 h. The impregnated solid was then collected by vacuum filtration in air, washed three times with 10 mL aliquots of mesitylene (97%, Aldrich), and dried under suction on the filter frit for 15 min. The impregnated and rinsed zeolite was then placed in an alumina boat ($10 \times 30 \times 107$ mm) which was inserted into a quartz tube (ø 45 mm) installed in a horizontal tube furnace (HST 12/600, Carbolite Gero). The tube was purged under dry argon flow (200 sccm) at ambient pressure. The FA within the zeolite pores was first polymerized by heating up to 80 °C via a 10 min ramp and held for 24 h. The poly-FA was then carbonized by heating up to 700 °C via a 2 h ramp and held for 30 min. Further carbon impregnation was accomplished via propylene CVD at 700 °C; the gas flow was switched to 7 mol% propylene in argon (99.99% propylene in 99.999% argon) at 200 sccm. After ambient-pressure CVD for 5 h, the gas flow was returned to dry argon at 200 sccm. An annealing step was performed by heating the zeolite-carbon composite up to 900 °C via a 1 h ramp, and held for an additional 1 h. The system was then cooled overnight, the gas flow was stopped, and the annealed zeolite-carbon composite was collected. Removal of the zeolite template was accomplished by three sequential dissolutions in 35 mL of aqueous hydrofluoric acid (HF, 40%, Sigma-Aldrich). The final ZTC product was collected by centrifugation, washed three times with 35 mL aliquots of distilled water, and then dried in air at 40 °C to obtain "archetypical **FAU**-ZTC."

1.2. Powder X-Ray Diffraction: Powder X-ray diffraction (XRD) measurements were performed on a Rigaku Ultima IV diffractometer using Cu Kα radiation ($\lambda = 1.54$ Å), generated at 40 kV and 40 mA, in Bragg-Brentano geometry. The powder was thinly dispersed on a "zero-background" sample holder comprised of oriented crystalline silicon. The data were analyzed by direct subtraction of the contribution from the sample holder determined by performing an identical experiment without any sample. The XRD pattern of archetypical **FAU**-ZTC is shown in **Figure S1**.
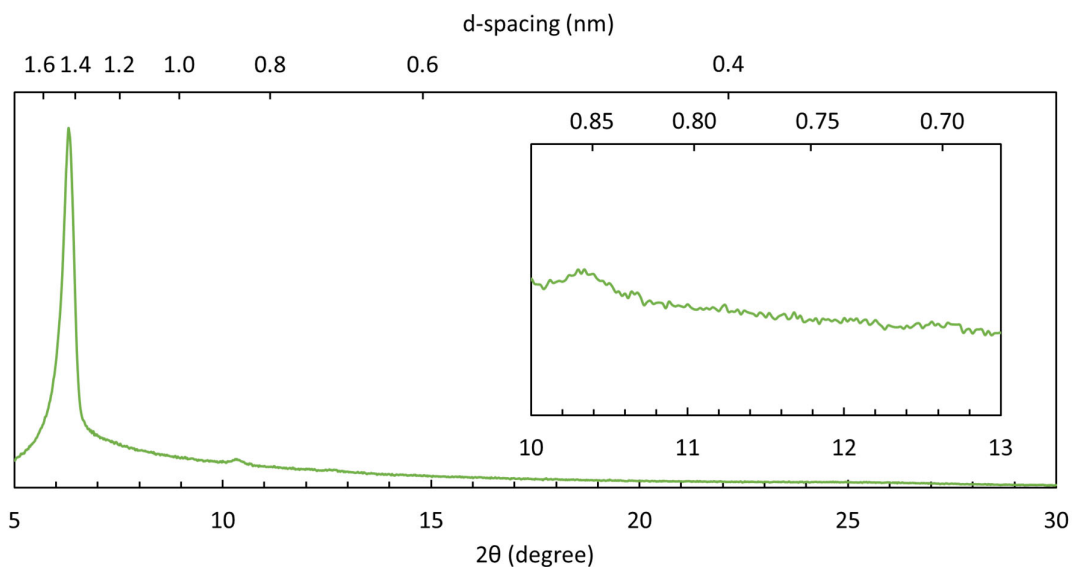
Figure S1. XRD pattern of archetypical **FAU**-ZTC.

1.3. Nitrogen Adsorption: Nitrogen adsorption/desorption isotherms were measured at 77 K between 10^{-4} and 100 kPa using an automated volumetric instrument (3Flex, Micromeritics Instrument Corp.). Specific surface areas were calculated by the Brunauer-Emmett-Teller (BET) method between $P/P_0 = 0.000004\text{-}0.11$. Pore-size distributions were determined by nonlocal density functional theory (NLDFT) calculations using a dedicated software package (MicroActive Share, Micromeritics Instrument Corp.) using a carbon slit-pore model. The nitrogen adsorption/desorption isotherm on archetypical **FAU**-ZTC is shown in **Figure S2**.
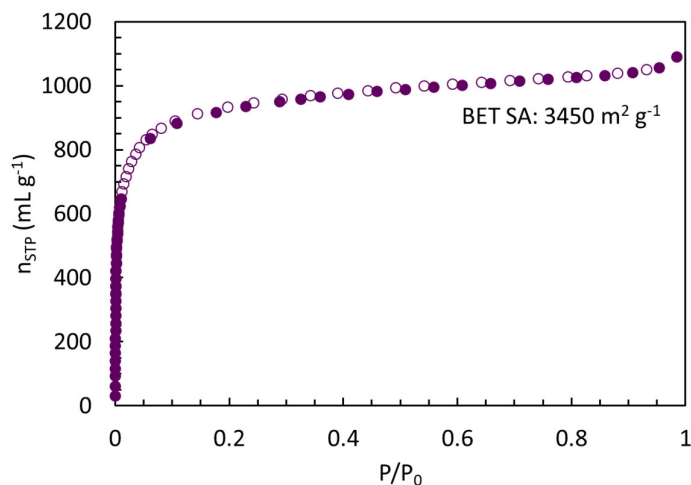

Figure S2. Equilibrium N_2 adsorption/desorption isotherm of archetypical **FAU**-ZTC at 77 K (filled/unfilled, respectively).

1.4. Thermal Gravimetric Analysis: Thermal gravimetry was performed using a micro-balance (Discovery TGA, TA Instruments) under flowing dry air (Grade D breathing air with moisture trap). Zeolite-carbon composite collected prior to HF treatment was suspended in the sample enclosure, and the typical starting sample weight was ~5 mg. The balance flow rate was 1.0 mL min^{-1} and the temperature program was specified as follows: the sample was first held at 50 °C for 15 min under dry air to purge, water removal was performed by heating up to 300 °C via a 20 °C min^{-1} ramp. The weight at the end of this dehydration step was taken to be the initial mass, m_i. The carbon was then oxidized by heating up to 800 °C via a 5 °C min^{-1} ramp and held for 120 min, and finally the remaining sample was cooled to 300 °C to determine the final weight difference. The weight change corresponding to the oxidation/removal of archetypical **FAU**-ZTC (within its native zeolite NaY template) is shown in **Figure S3**.
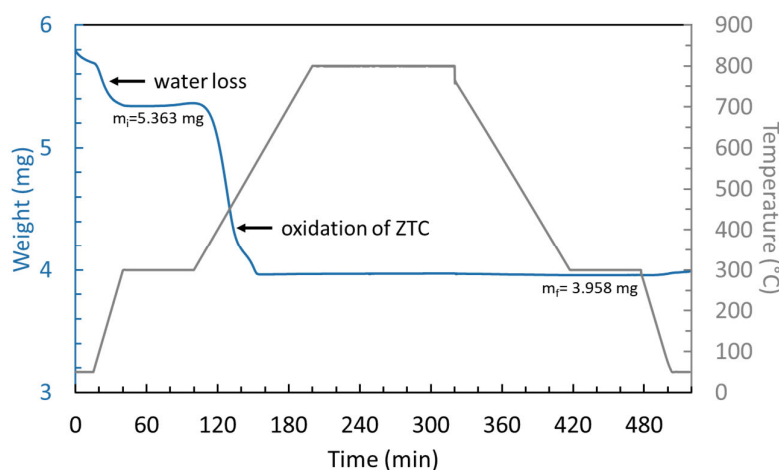

Figure S3. Thermal gravimetric analysis of archetypical FAU-ZTC. Three regions of weight loss are observed: water loss at 50 °C during purge (0-12 min), water loss between 50-300 °C (12-42 min), and oxidation of ZTC above 300 °C (87-158 min).

2. Experimental Structural Packing Density (SPD)

Equations 1-3 in the main text define three metrics of evaluation for the comparison of ZTC structure density (including carbon along with hydrogen and oxygen) packing within the zeolite template, a key indicator of both the template fidelity and structure of the final ZTC product after removal of the template. Analysis of the raw thermal gravimetry measured for archetypical **FAU**-ZTC is shown in **Figure S3**. The weight loss corresponding to the weight of the carbonaceous ZTC occurs above 300 °C, after a clear plateau is achieved following the low-temperature weight loss associated with adsorbed water.

The calculations of SPD_{exp}, SPD_{cell}, and $SPD_{cell,vol}$ for archetypical **FAU**-ZTC (corresponding to the measurement in **Figure S3**) are as follows:

$$SPD_{exp} = \frac{5.363 \text{ mg} - 3.958 \text{ mg}}{3.958 \text{ mg}} = 0.355 \text{ g}_C \text{ g}_{zeolite}^{-1} \qquad \text{Equation S1}$$

$$SPD_{cell} = 0.355 \text{ g}_C \text{ g}_{zeolite}^{-1} \times \frac{494.38 \text{ g}_{zeolite}}{450.6 \text{ g}_{SiO_2}} = 0.39 \text{ g}_C \text{ g}_{SiO_2}^{-1} \qquad \text{Equation S2}$$

$$SPD_{cell,vol} = 0.389 \text{ g}_C \text{ g}_{SiO_2}^{-1} \times 1.327 \text{ g SiO}_2 \text{ cm}^{-3} = 0.52 \text{ g}_C \text{ cm}^{-3} \quad \text{Equation S3}$$

3. Theoretical X-Ray Diffraction Pattern Simulation

Powder XRD patterns were simulated for each of the periodic atomistic models of **FAU**-ZTC using openly accessible software (Mercury, v4.1.3, Cambridge Crystallographic Data Centre) using a simulated wavelength of 1.54056 Å, a step size of $2\theta = 0.02°$, and a full-width half-maximum (FWHM) of $2\theta = 0.1°$.[S1] The results are shown in **Figure 12** in the main text. The angles corresponding to the (111) and (220) reflections are tabulated in **Table S1**.

Table S1. Experimental and Theoretical XRD Reflections of **FAU**-ZTC.

Model/Material	(111)	(220)
Roussel Model 2006	6.16	10.06
Nishihara Model 0a 2009	6.31	10.32
Nishihara Model 0b 2009	5.80	9.48
Nishihara Model I 2009	6.36	8.99
Kim Model 2016	6.11	9.98
Nishihara Model II 2018	6.36	10.39
Braun Model NR 2018	6.11	9.98
Braun Model R 2018	5.98-6.09	11.42-11.68
Tanaka Model IV 2018	6.36	10.39
Archetypical **FAU**-ZTC	6.32	10.40
Tosoh Zeolite NaY	6.28	10.26

4. Theoretical Surface Area and Pore Size Distribution

Nitrogen accessible surface area calculations were performed using openly accessible software (Zeo++, v.0.3, http://www.zeoplusplus.org/) assuming a channel radius and probe radius of 2.27 Å (corresponding to N_2) with 2000 Monte Carlo samples per atom.[S2] The results are shown in **Table 2** in the main text. Likewise, pore-size distributions were simulated using the same assumptions except with 50000 Monte Carlo samples per atom. The pore-size distributions for each model compared to archetypical **FAU**-ZTC (determined using NLDFT analysis of N_2 adsorption measurements at 77 K) are shown in **Figure S4**.
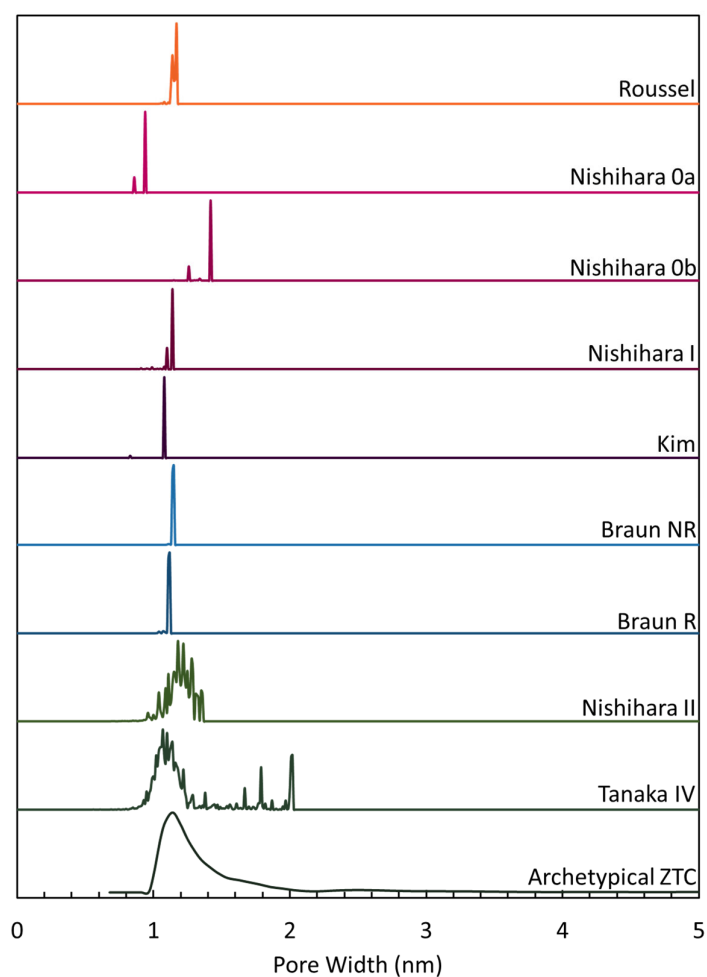

Figure S4. Experimental and theoretical N_2-accessible pore-size distributions for all periodic **FAU**-ZTC models and archetypical **FAU**-ZTC.

5. Theoretical Structural Packing Density

Structural packing densities were calculated for all of the periodic atomistic models of **FAU**-ZTC by determining the number (and mass) of all atoms within the unit cell per unit cell volume using the reported crystallographic information file (CIF) or molecular coordinate file for each structure. Then, based on the density of ideal SiO_2 faujasite (framework type **FAU,** International Zeolite Association) of 1.327 g mL^{-1}, the volumetric $SPD_{cell,vol}$ was converted to a gravimetric quantity, SPD_{cell}, in units of $g_C\ g_{SiO_2}^{-1}$. As noted in the main text, these units nominally imply that the mass of **FAU**-ZTC is comprised solely of "carbon" despite that some of the models as well as the real ZTC materials are actually comprised of C, H, and O. We emphasize that in the case of the models, values for SPD_{cell} and $SPD_{cell,vol}$ include contributions from all atoms in the unit cell of that model.

Table S2. Theoretical Structural Packing Densities.

Model	per Unit Cell				
	Carbon Atoms	Mass (Da)	Volume (nm³)	$SPD_{cell,vol}$ ($g_C\ cm^{-3}$)	SPD_{cell} ($g_C\ g_{SiO_2}^{-1}$)
Roussel Model 2006	630	7569	15.34	0.82	0.62
Nishihara Model 0a 2009	728	8746	14.23	1.02	0.77
Nishihara Model 0b 2009	272	3268	9.16	0.59	0.45
Nishihara Model I 2009***	288	3460	13.95	0.41	0.32
Nueangnoraj Model 2013	970	11654	27.00	0.54	0.72
Kim Model 2016*	217	2535	15.71	0.28	0.21
Kim Model 2016**	1202	14008	15.71	1.53	1.15
Nishihara Model II 2018***	2351	28245	111.56	0.94	0.33
Braun Model NR 2018	186	2235	3.93	0.91	0.71
Braun Model R 2018	186	2235	4.09	0.83	0.68
Tanaka Model IV 2018	8937	107369	376.40	0.47	0.36
Boonyoung Model 2019	200	2403	25.60	1.60	1.21

*partial occupation of lattice sites
**full occupation of lattice sites
***hydrogen included

A representative calculation of SPD_{cell} and $SPD_{cell,vol}$ for a carbon-only model (in this case, the Roussel Model) is shown below:

$$SPD_{cell,vol} = \frac{1.257 \times 10^{-20} \text{ g C}}{1.534 \times 10^{-20} \text{ cm}^3} = 0.82 \text{ g}_C \text{ cm}^{-3} \qquad \text{Equation S4}$$

$$SPD_{cell} = 0.82 \text{ g}_C \text{ cm}^{-3} \times 0.753 \text{ cm}^3 \text{ g}_{SiO_2}^{-1} = 0.62 \text{ g}_C \text{ g}_{SiO_2}^{-1} \quad \text{Equation S5}$$

Likewise, a representative calculation of SPD_{cell} and $SPD_{cell,vol}$ for a carbon- and hydrogen-bearing model (in this case, Nishihara Model II) is shown below:

$$SPD_{cell,vol} = \frac{5.746 \times 10^{-21} \text{ g C} + 1.208 \times 10^{-22} \text{ g H}}{1.395 \times 10^{-20} \text{ cm}^3} = 0.42 \text{ g}_{ZTC} \text{ cm}^{-3} \qquad \text{Equation S6}$$

$$SPD_{cell} = 0.42 \text{ g}_{ZTC} \text{ cm}^{-3} \times 0.753 \text{ cm}^3 \text{ g}_{SiO_2}^{-1} = 0.32 \text{ g}_C \text{ g}_{SiO_2}^{-1} \quad \text{Equation S7}$$

6. Manipulation of the Atomistic Models

For comparison of the atomistic models reported by several different research groups over the time period between 2007-2019, it was necessary to obtain or create a crystallographic information file (CIF) for each model that could be used for XRD pattern simulation and surface area and pore-size distribution calculations. Of the ten models reviewed herein, one molecular coordinate file (XYZ file) and three CIFs were obtained directly from the published literature (the Boonyoung, Kim, and Braun Models, respectively), and three molecular coordinate files (XYZ and PBD files) and five CIFs were obtained directly from their authors and used with the authors' permission (the Nueangnoraj, Roussel, Nishihara, and Tanaka Models). Since the Roussel, Nueangnoraj, and Boonyoung models only existed as molecular coordinate files, an effort was made herein to generate CIFs from the original files. A CIF was generated from the molecular coordinate file provided for the Roussel model. However, it was determined that the Nueangnoraj Model and Boonyoung Model were too distorted and too small, respectively, to generate a CIF that would accurately replicate the reported model's structure.

All of the models reviewed in this work are shown in detail in **Figures S5-S20**. Several of the models have multiple variants, as explained in the main text. The figures depict (a) a *representative* section of connectivity between two "nodes" of the **FAU**-ZTC structure, formed within and between two supercages of the original **FAU** zeolite framework, and (b) an extended multi-cell depiction of the **FAU**-ZTC structure showing pore-to-pore regularity with a repeat distance of ~1.4 nm (corresponding to the dominant (111) reflection given in **Table S1**). Structural files of all models are available as additional supporting information in this work.
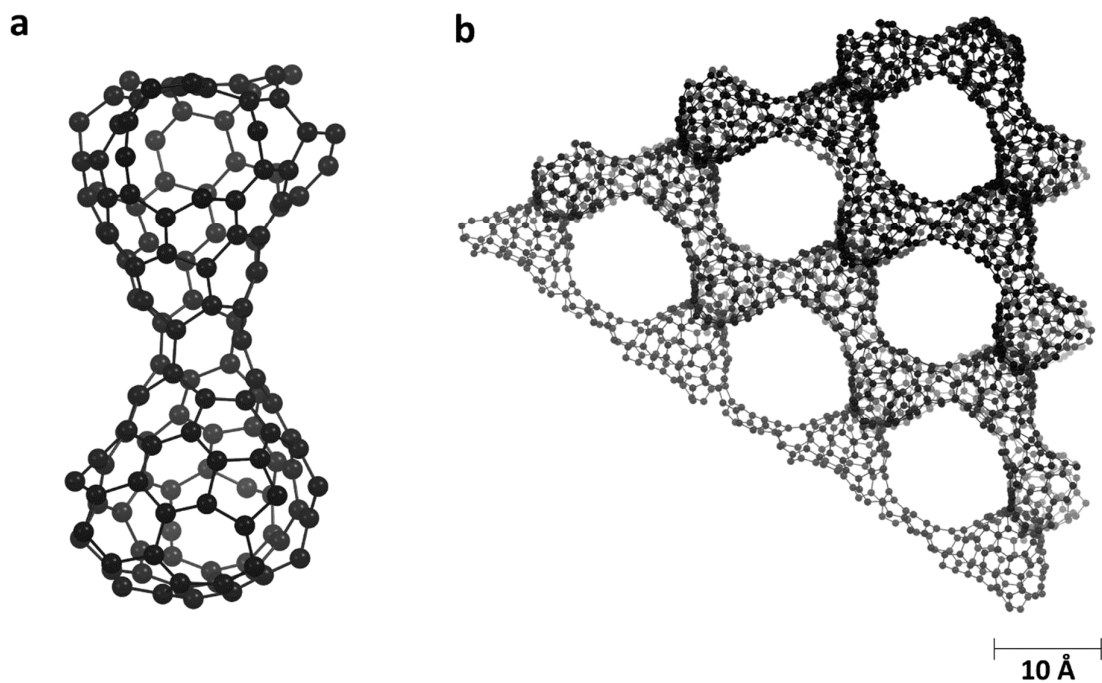
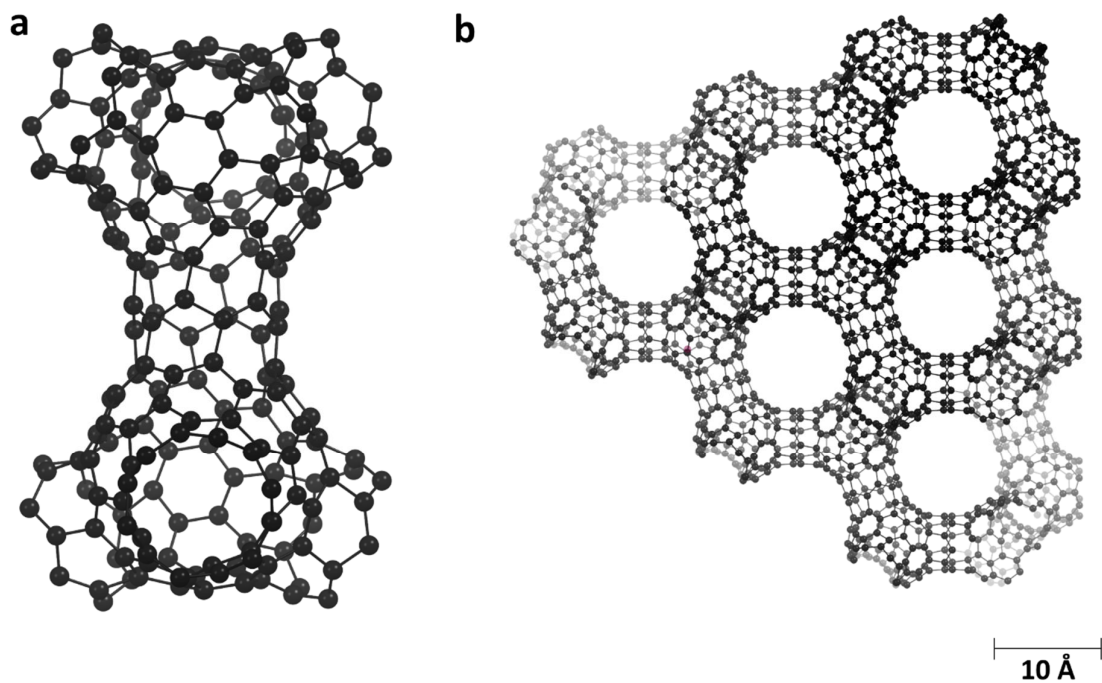**Figure S5.** Roussel Model (2006): (a) a two-cell closed-strut subunit and (b) an extended multi-cell structure.

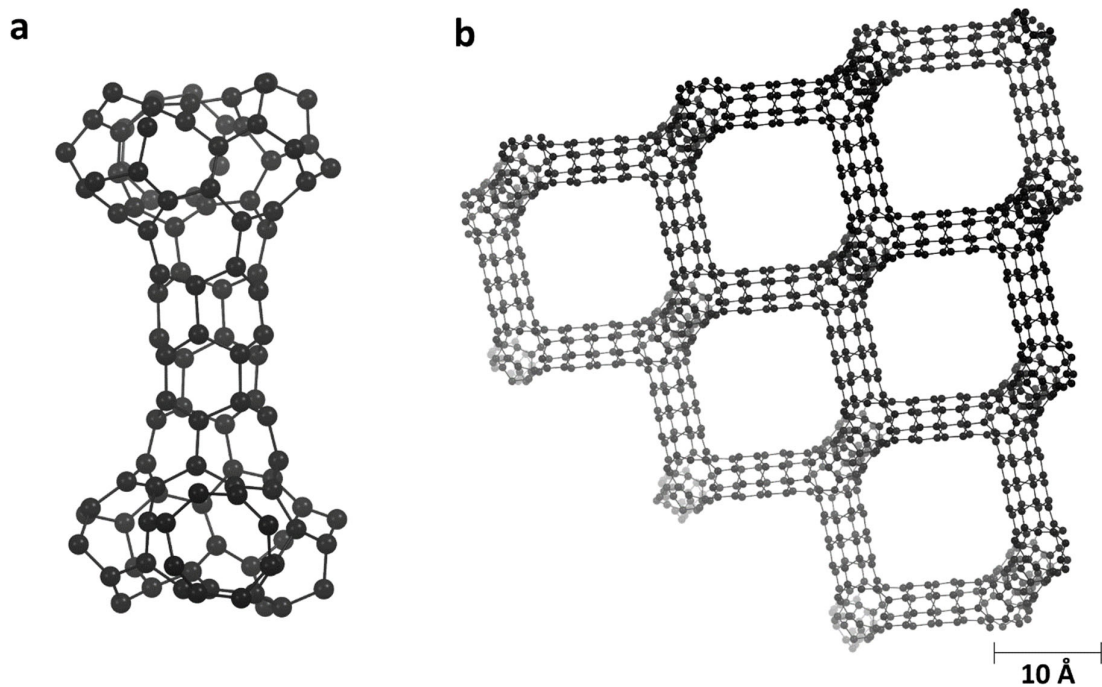**Figure S6.** Nishihara Model 0a (2009): (a) a two-cell closed-strut subunit and (b) an extended multi-cell structure.

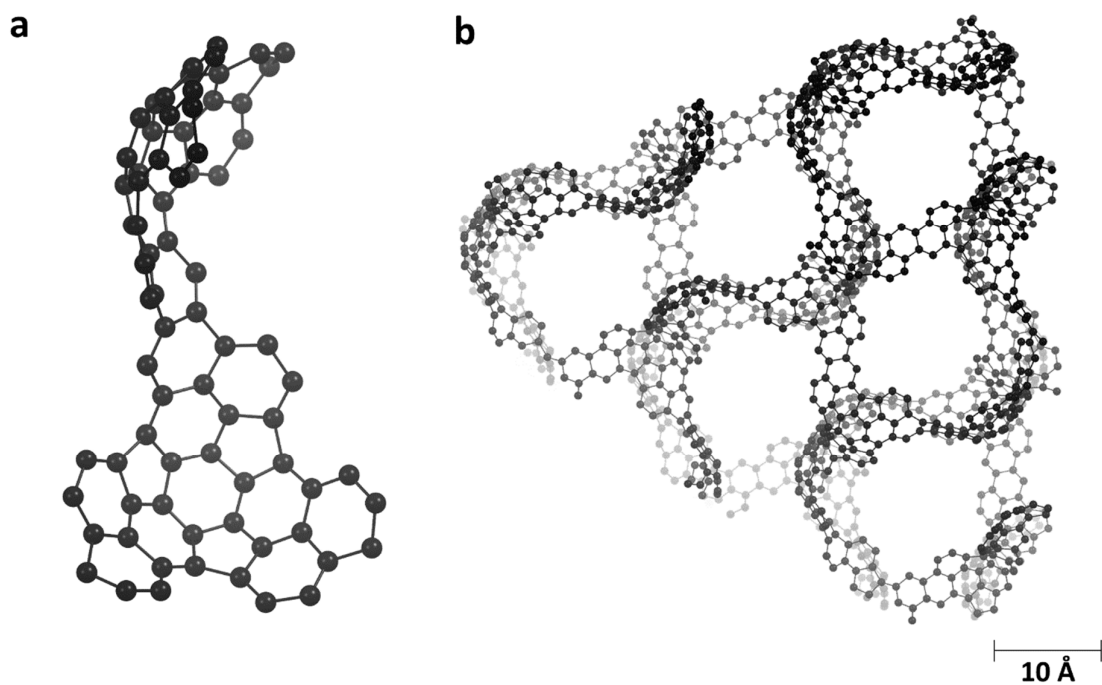**Figure S7.** Nishihara Model 0b (2009): (a) a two-cell closed-strut subunit and (b) an extended multi-cell structure.

Figure S8. Nishihara Model I (2009): (a) a two-cell open-blade "buckybowl" subunit and (b) an extended multi-cell structure. Hydrogen is excluded for clarity.
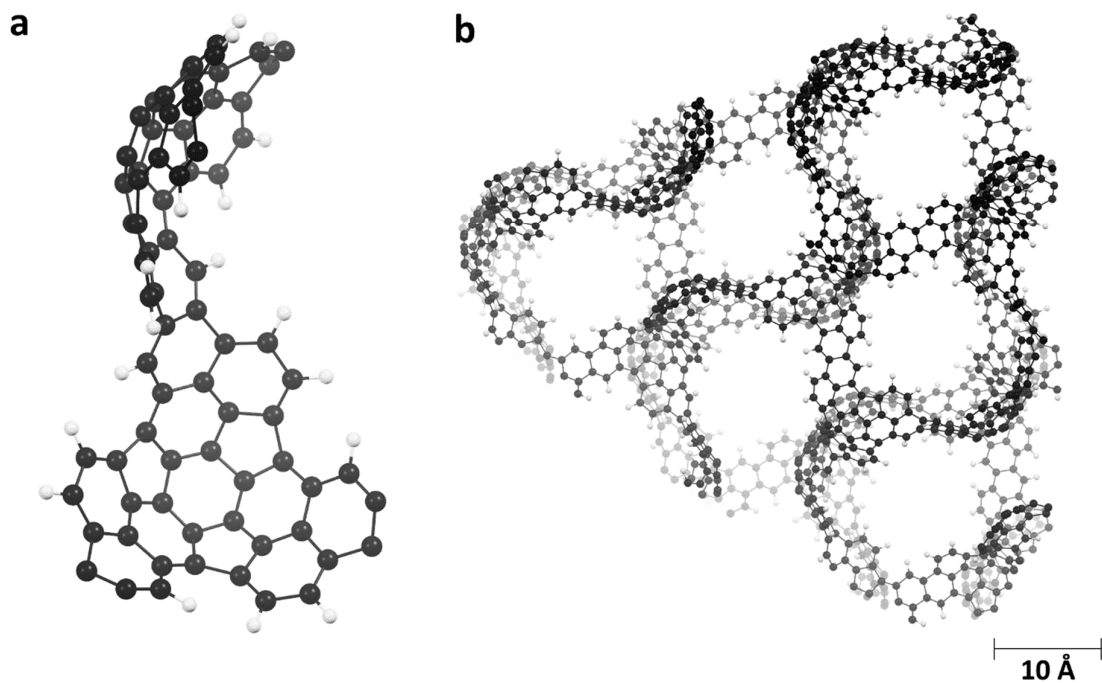
Figure S9. Nishihara Model I (2009): (a) a two-cell open-blade "buckybowl" subunit and (b) an extended multi-cell structure. Hydrogen is shown in white.
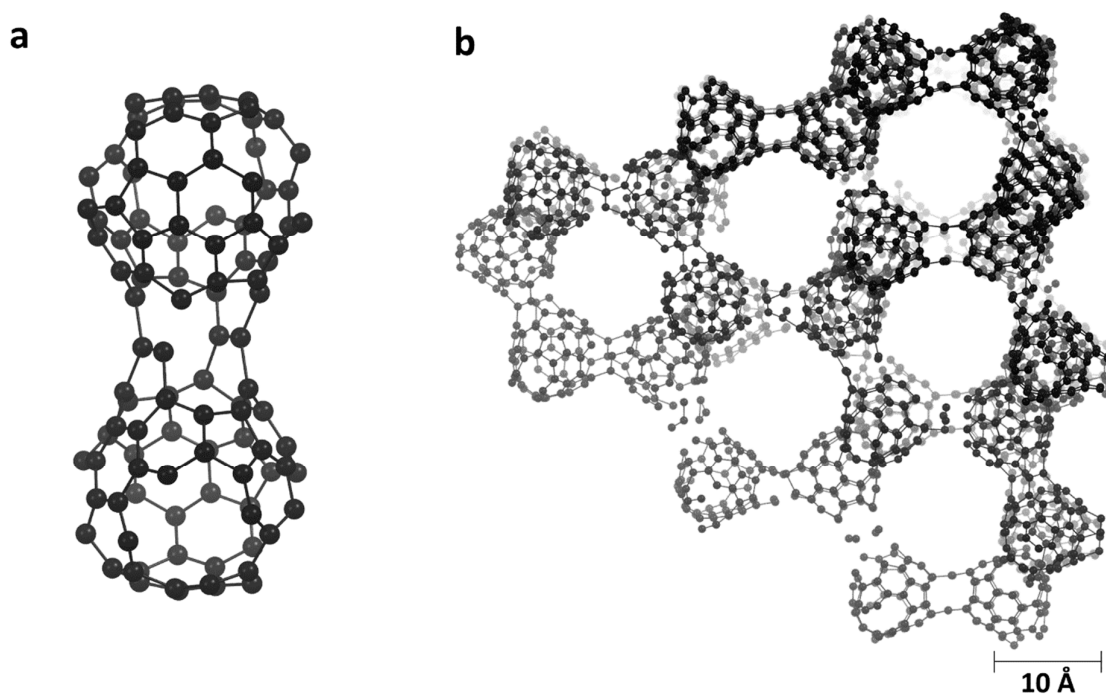

Figure S10. Nueangnoraj Model (2013): (a) a two-cell closed-strut fullerene-like subunit and (b) an extended multi-cell structure.
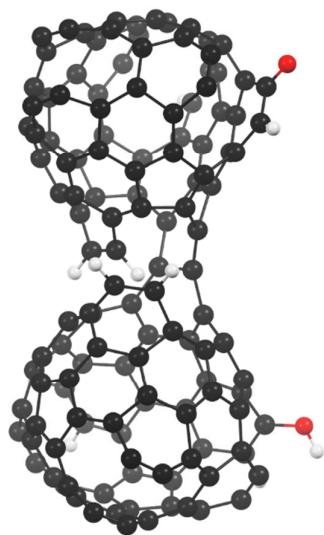
Figure S11. Nueangnoraj Model (2013): a two-cell closed-strut fullerene-like subunit with oxygen shown in red and hydrogen shown in white.
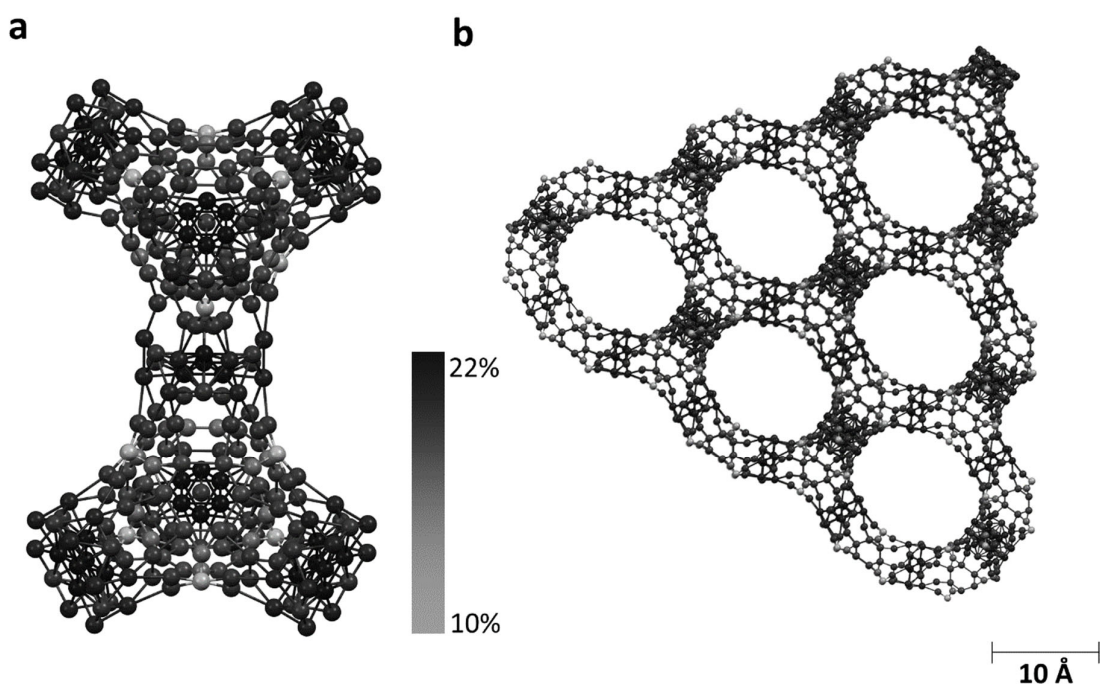

Figure S12. Kim Model (2016): (a) tetrahedrally-coordinated "closed-strut" subunit with partial occupancy on each lattice site (probability of occupation indicated by shading from dark grey, 22%, to white, 10%) and (b) an extended multi-cell structure.
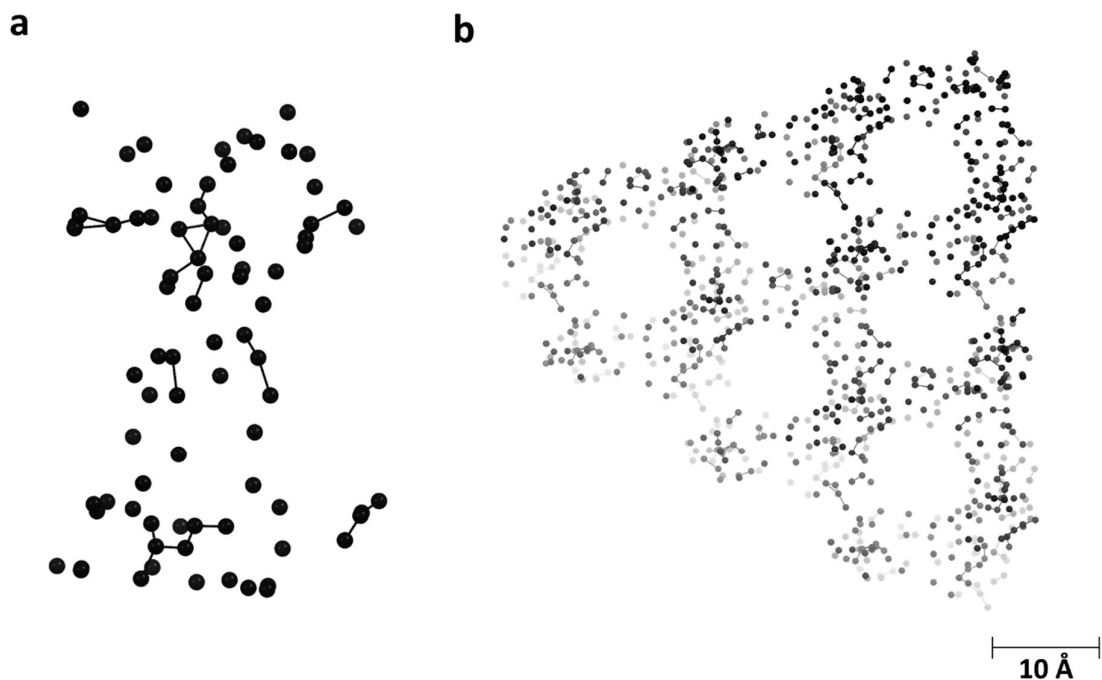
Figure S13. Kim Model (2016): (a) a representative subunit with partial occupancy on each lattice site and (b) an extended multi-cell structure.
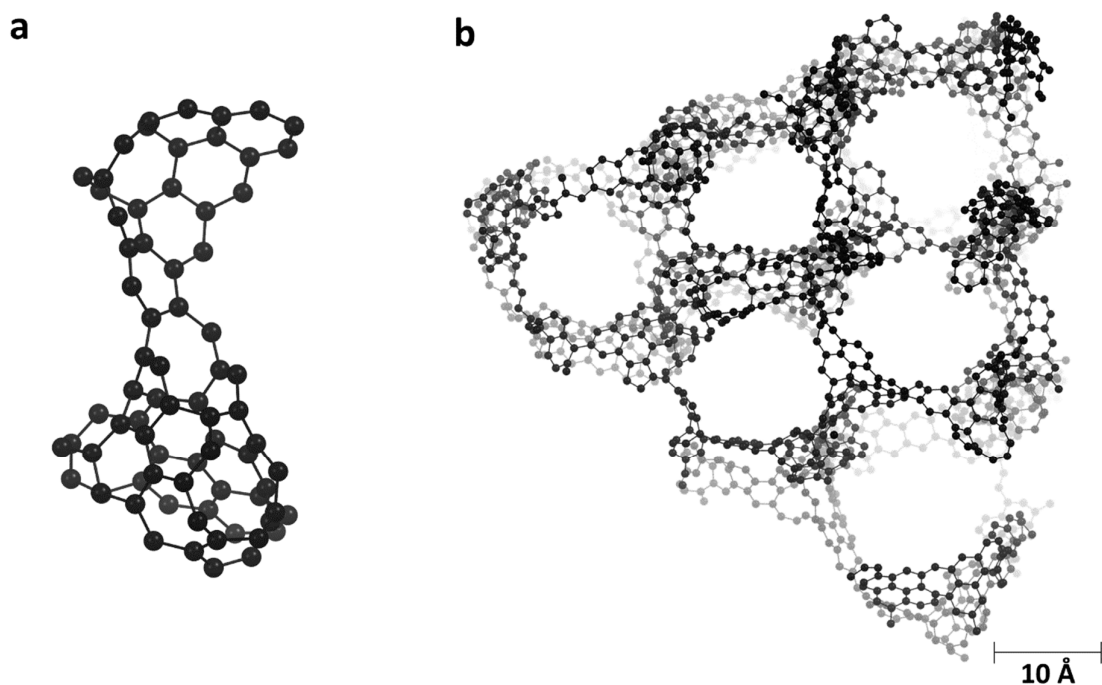

Figure S14. Nishihara Model II (2018): (a) a representative two-cell open-blade subunit (out of 36 different subunits within the 2×2×2 supercell) and (b) an extended multi-cell structure. Hydrogen is excluded for clarity.

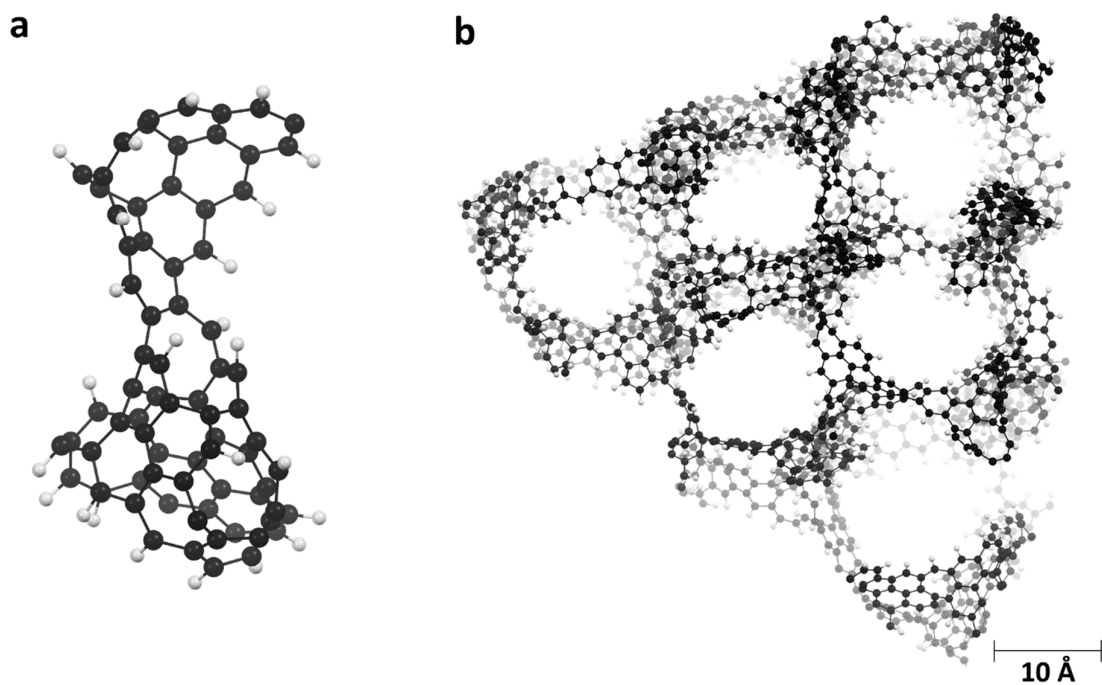**Figure S15.** Nishihara Model II (2018): (a) a representative two-cell open-blade subunit (out of 36 different subunits within the 2×2×2 supercell) and (b) an extended multi-cell structure. Hydrogen is shown in white.

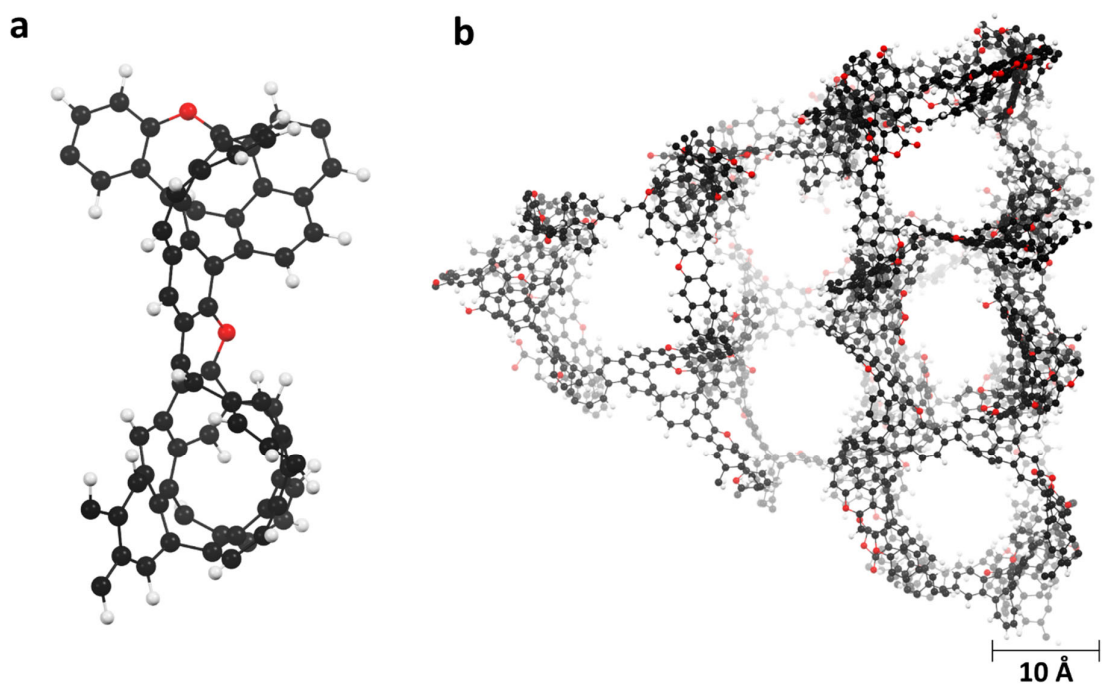**Figure S16.** Nishihara Model II (2018): (a) a representative two-cell open-blade subunit (out of 36 different subunits within the 2×2×2 supercell) and (b) an extended multi-cell structure. Oxygen and hydrogen are shown in red and white, respectively.
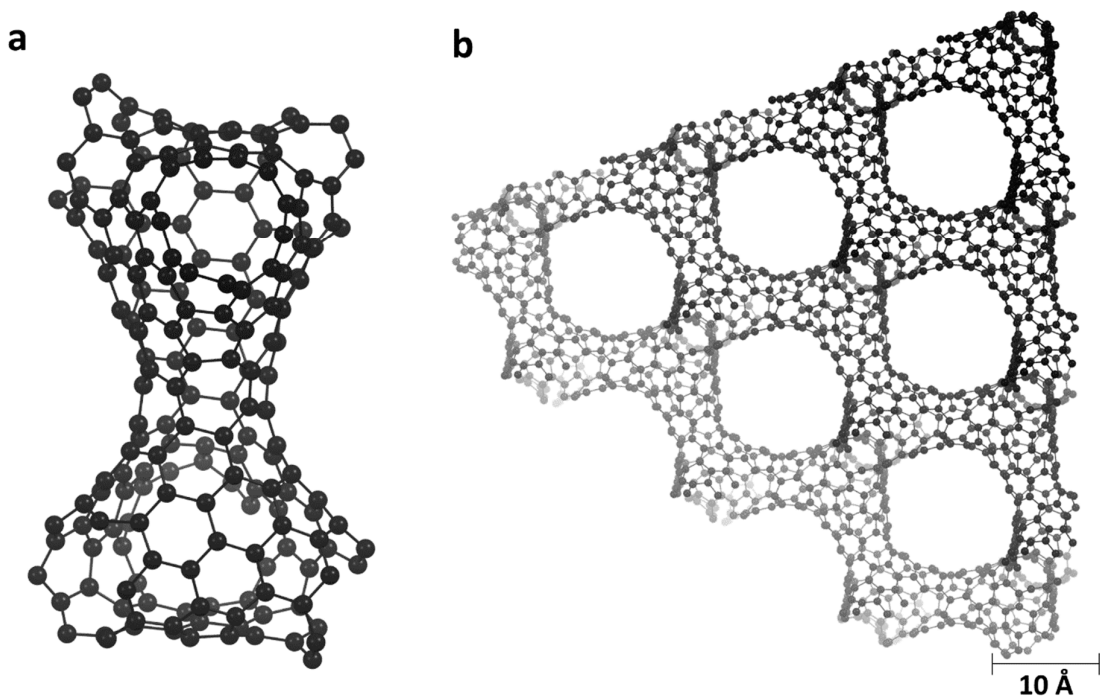
Figure S17. Braun Model NR (2018): (a) tetrahedrally-coordinated, negatively curved "closed-strut" subunit and (b) an extended multi-cell structure.
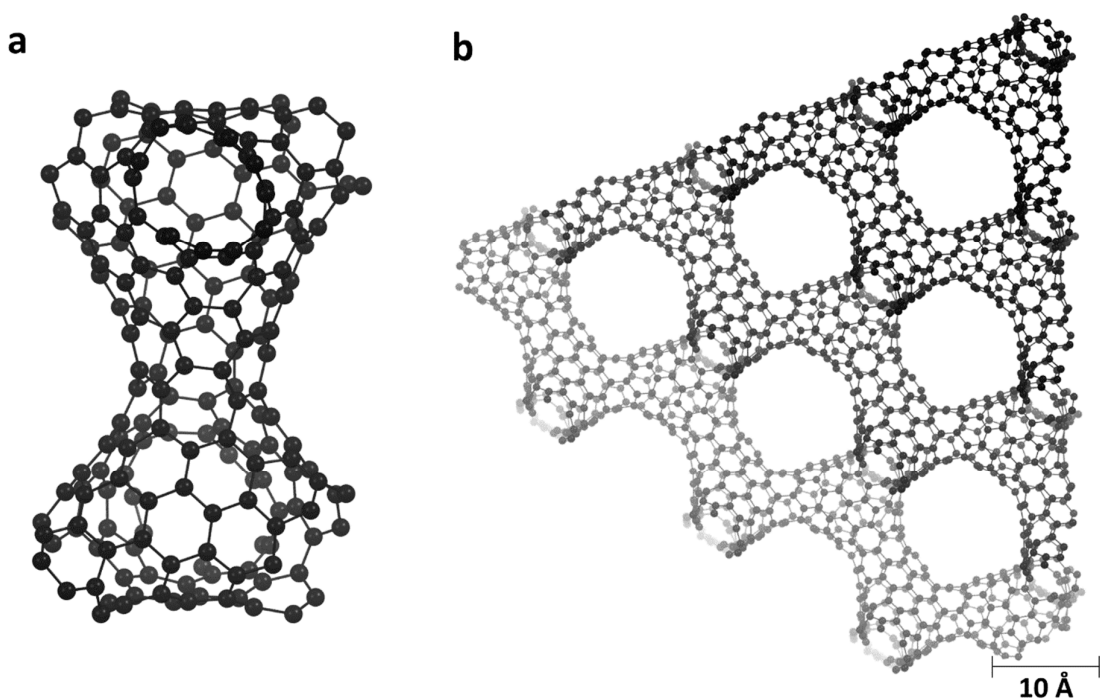
Figure S18. Braun Model R (2018): (a) tetrahedrally-coordinated, negatively curved "closed-strut" subunit and (b) an extended multi-cell structure, after structural relaxation.

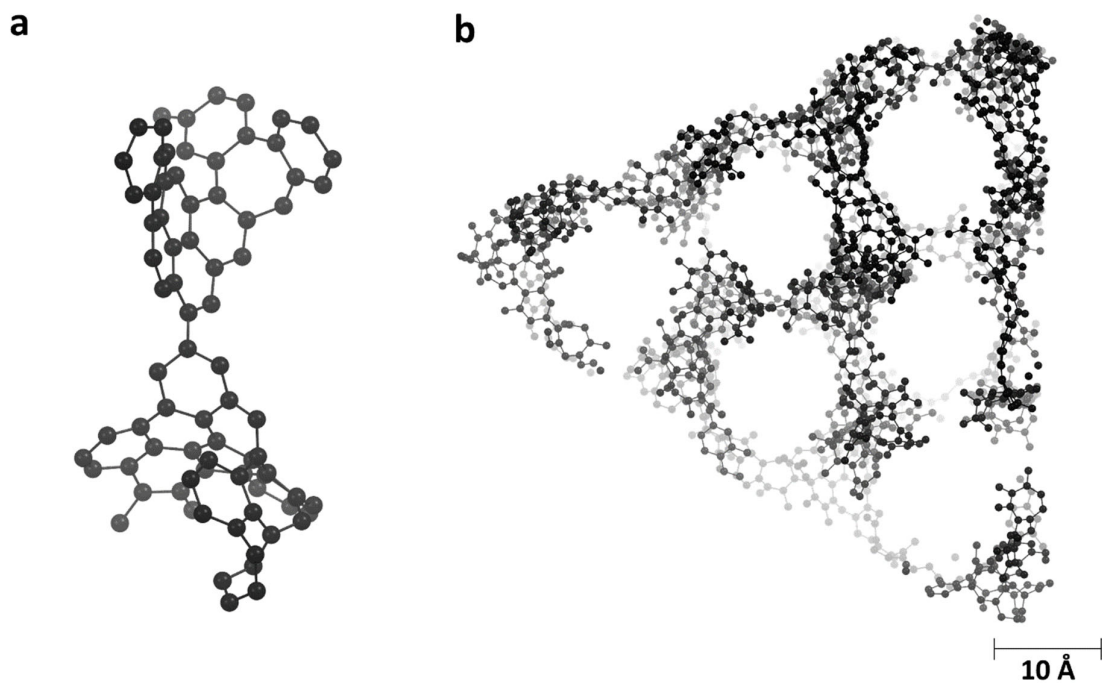**Figure S19.** Tanaka Model IV (2018): (a) a representative two-cell open-blade subunit (out of 100 different subunits within the 3×3×3 supercell) and (b) an extended multi-cell structure.
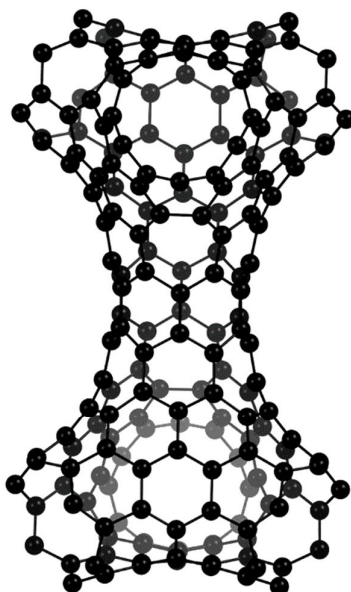

Figure S20. Boonyoung Model (2019): tetrahedrally-coordinated "closed-strut" subunit.

7. Examination of Claims of Braun and Coworkers

In recent work, Braun and coworkers claimed to "establish" that currently synthesized ZTCs can be modeled and understood as a form of schwarzite.[S3] Several of their key claims are reproduced below:

> "As we will show, the similarity between ZTCs and schwarzites is striking, and we explore this similarity to establish that the theory of schwarzites/TPMSs is a useful concept to understand ZTCs." (page 1)[S3]

> "In this work, we develop an improved molecular description of ZTCs, show that they are equivalent to schwartzites [sic], and thus make the experimental discovery of schwarzites ex post facto." (page 1) [S3]

> "Although schwarzites have been a purely hypothetical concept, our work suggests that ZTCs are schwarzites incarnate." (page 6) [S3]

In the analysis performed in this review, it has been clearly shown that none of the models proposed by Braun and coworkers represent archetypical **FAU**-ZTC. The simulated XRD pattern of the Braun Model exhibits multiple peaks above 12° which have not been observed for archetypical **FAU**-ZTC or any other carbon synthesized inside a zeolite template. Furthermore, the simulated surface area of the Braun Model is 1440-1480 $m^2\,g^{-1}$, closer to that of a one-sided graphene sheet than that of archetypical **FAU**-ZTC. The very high surface area of well-replicate ZTCs synthesized in the laboratory are indicative of open-blade structures as opposed to closed-tube structures like the Braun Model. Lastly, the calculated SPD of the Braun Model is roughly twice that of archetypical **FAU**-ZTC when careful consideration of the nature of the zeolite template is taken. It should also be noted that the Braun Model and all other carbon-only models are highly misrepresentative of the actual chemical composition of laboratory-synthesized ZTCs which contain a very high content of hydrogen (a factor that distinguishes ZTCs from activated carbons) as well as oxygen.

Braun and coworkers incorrectly claim:

> "We have developed a theoretical framework to generate a ZTC model from any given zeolite structure, which we show can successfully predict the structure of known ZTCs." (abstract)[S3]

> "Our method correctly describes the structures of the known ZTCs…" (page 6)

> "[T]his library should serve to ... provide computational scientists
> with realistic atomistic models." (page 6)[S3]

> "Indeed, the experimental properties of ZTCs are exactly those which
> have been predicted for schwarzites..." (page 1)[S3]

We emphasize that while the above claims are factually incorrect, all of the models reported in their work are interesting purely for fundamental reasons; they represent hypothetical schwarzite materials that *could* be synthesized within a zeolite template under the correct synthetic conditions.

It is important to note that Braun and coworkers were not the first to establish a hypothetical link between ZTCs and schwarzites. This link is attributed both to Kyotani and coworkers over many years in their research, as well as Roussel and coworkers who first published this idea in 2007.[S4] Furthermore, the models reported by Braun and coworkers should be more accurately defined as "non-balanced" schwarzites since they do not separate space into two identical volumes. Two examples of false claims as to the novelty of the link between ZTCs and schwarzites as presented in 2019 are reproduced below:

> "[O]ur results establish the relationship between ZTCs and
> schwarzites—carbon materials with negative Gaussian curvature that
> resemble TPMSs—linking the research topics and demonstrating that
> schwarzites should no longer be thought of as purely hypothetical materials." (page 1)[S3]

> "[W]e have shown how ZTCs can be associated with TPMSs, linking
> the research topics of ZTCs and schwarzites." (page 6)[S3]

While the Braun models retain importance as idealized hypothetical schwarzites that may eventually be synthesized in the laboratory under conditions still unknown to the experimental community, the above false claims are already leading to very important, erroneous misrepresentations of ZTCs in recent reports by other researchers. The following are several examples of mistaken depictions of the Braun models as accurate representations of experimental ZTCs, or of the general conclusion that ZTCs are now to be classified as schwarzites.

> "UC Berkeley chemists have proved that three carbon structures recently created by scientists in South Korea and Japan are in fact the
> long-sought schwarzites..." (paragraph 2)[S5]

"... (zeolite-templated carbons) were being investigated for possible interesting properties, though the creators were unaware of their identity as schwarzites, which theoretical chemists have worked on for decades." (paragraph 3)[S5]

"The team determined that, of the approximately 200 zeolites created to date, only 15 can be used as a template to make schwarzites, and only three of them have been used to date to produce schwarzite ZTCs." (paragraph 17)[S5]

"It has been recently reported that the growth of carbon inside the hard porous materials, so-called template carbonization, has successfully synthesized carbons with structures that fits the description of schwarzites." (page 1)[S6]

"Recently, Braun et al. developed a theoretical framework to generate a ZTC model from any given zeolite structure, predicting the structure of known ZTCs..." (page 93)[S7]

"... a 3D graphene that maintains the unique electronic properties of planar graphene... can be achieved via templating strategies... as suggested computationally via zeolite templating." (page 5)[S8]

"[R]ecently, Braun et al. developed an efficient computational approach to generate an accurate ZTC structure at atomic levels in agreement with experiment data." (page 2)[S9]

"In ZTC which is recognized as schwarzite, sp^2 carbon surface divides a structure into two disjoint spaces which don't exchange molecules." (page 4)[S9]

8. Supporting References

S1.   Macrae, C. F.; Edgington, P. R.; McCabe, P.; Pidcock, E.; Shields, G. P.; Taylor, R.; Towler, M.; Streek, J. V. D., Mercury: visualization and analysis of crystal structures. *J. Appl. Crystallogr.* **2006,** *39* (3), 453-457.

S2.   Willems, T. F.; Rycroft, C. H.; Kazi, M.; Meza, J. C.; Haranczyk, M., Algorithms and tools for high-throughput geometry-based analysis of crystalline porous materials. *Micropor. Mesopor. Mat.* **2012,** *149* (1), 134-141.

S3.   Braun, E.; Lee, Y.; Moosavi, S. M.; Barthel, S.; Mercado, R.; Baburin, I. A.; Proserpio, D. M.; Smit, B., Generating carbon schwarzites via zeolite-templating. *Proc. Natl. Acad. Sci. U.S.A.* **2018**, 115 (35), E8116-E8124.

S4.   Roussel, T.; Didion, A.; Pellenq, R. J.-M.; Gadiou, R.; Bichara, C.; Vix-Guterl, C., Experimental and Atomistic Simulation Study of the Structural and Adsorption Properties of Faujasite Zeolite-Templated Nanostructured Carbon Materials. *J. Phys. Chem. C* **2007**, 111, 15863-15876.

S5.   Sanders, R. (2018, August 13). *Long-sought carbon structure joins graphene, fullerene family*. Retrieved from https://news.berkeley.edu/2018/08/13/long-sought-carbon-structure-joins-graphene-fullerene-family/

S6.   Boonyoung, P.; Kasukabe, T.; Hoshikawa, Y.; Berenguer-Murcia, Á.; Cazorla-Amorós, D.; Boekfa, B.; Nishihara, H.; Kyotani, T.; Nueangnoraj, K., A Simple "Nano-Templating" Method Using Zeolite Y Toward the Formation of Carbon Schwarzites. *Front. Mater.* **2019**, 6, 104.

S7.   Nicolaea, S. A.; Wangb, X.; Hedinb, N.; Titiricia, M.-M., Refined biocarbons for gas adsorption and separation. *Green Carbon European Training Network* **2019**, 83.

S8.   Martin, J. W.; de Tomas, C.; Suarez-Martinez, I.; Kraft, M.; Marks, N. A., Topology of disordered 3D graphene networks. *Phys. Rev. Lett.* **2019,** *123* (11), 116105.

S9.   Cui, J.; Zhang, K.; Zhang, X.; Lee, Y., A computational study to design zeolite-templated carbon materials with high performance for CO_2/N_2 separation. *Micropor. Mesopor. Mat.* **2019**, 109947.